SEASONAL STUDY OF DIRECTIONAL REFLECTANCE PROPERTIES OF SNOW

Daniel Odermatt[1], Daniel Schläpfer[1], Michael Lehning[2], Margit Schwikowski[3], Matthias Kneubühler[1] and Klaus I. Itten[1]

1. Remote Sensing Laboratories (RSL), University of Zurich, Department of Geography, Zurich, Switzerland; daniodermatt(at)hotmail.com
2. WSL, Swiss Federal Institute for Snow and Avalanche Research SLF, Davos, Switzerland; lehning(at)slf.ch
3. Paul Scherrer Institute, Villigen, Switzerland; margit.schwikowski(at)psi.ch

ABSTRACT

We present an analysis of the hemispherical-directional reflectance factor (*HDRF*) of snow, using 16 seasonal datasets of the spectral range from 400 to 2,500 nm. The data was measured under clear sky conditions in Davos Dorf (Grisons, Switzerland, 1,560 m a. s. l.). Fieldwork was carried out on seven days between February 5 and March 30 2004 with the Swiss Field Goniometer System (FIGOS). In addition to the *HDRF* measurements, snow stratigraphy, temperature and density were measured, and chemical and photomicroscopical analyses of snow samples were performed. Concentration of organic and elemental carbon was determined by chemical analysis. The grain size analyses through image processing of micrographs revealed relatively small differences of 0.21 to 0.33 mm mean radius in the top layers of snow cover. Seven datasets present *HDRF* of wet snow surfaces with similar anisotropy at smaller sun zenith angles (θ_l =3.3 to 64.5°) compared to the nine surfaces measured at larger sun zenith angles (θ_l =6.5 to 75.3°). Spectral albedo is relatively constant throughout datasets of different sun zenith angles of the same day, but has large variability among measurements of different days. With increasing wavelength, it decreases significantly faster for wet surfaces than for dry surfaces. The forward scattering peak was found to strengthen with increasing sun zenith angle and with increasing wavelength for both wet and dry surfaces at wavelengths above 700 nm. Finally, a spectral wet snow determination method is performed and the cross-sensitivity to *HDRF* variation could be derived. The best differentiability was found for 1,380 nm. This basis work increases the understanding of snow signatures for potential imaging spectroscopy applications in alpine regions.

Keywords: Snow HDRF, snow albedo, field goniometry.

INTRODUCTION

Knowledge of the directional reflectance of alpine snow cover is needed to improve retrieval of earth surface physical properties in general and snow physical properties in particular by air- and space borne remote sensing. It enables directional reflectance inversion models to be validated and energy balance models to be improved. The hemispherical-directional reflectance factor (*HDRF*) (1) of snow is influenced by snow texture, grain morphology, solar zenith angle, liquid water content, impurity concentration and surface roughness (2). In recent work regarding this subject, small goniometry devices and spectroradiometers have been used to quantify *HDRF* (2,3). They present 3 and 4 datasets with sun zenith angles θ_l =41 to 48° and θ_l =54 to 57°, respectively. Painter and Dozier (2) found a small local backscattering peak for fine-grained snow only but increased reflectance for all wavelengths in the forward half of the solar principal plane. Their comparison of surfaces of different grain sizes shows that the increase of single-scattering co-albedo with wavelength and grain size causes higher anisotropy. Aoki et al. (3) determined snow impurities as materials of soil origin and a smaller part of aerosols from fuel burning and quantified their impact on reflectance. Painter and Dozier (2) as well as Aoki et al. (3) finally compare their field data to the results of radiative transfer models. Measurements at a broader range of sun zenith angles (θ_l =67° to 90°) are presented in a third study focussing on the surface roughness caused

by sastrugi (4). A strong increase of forward scattering is observed for large zenith angles. An overview of *HDRF* measurements on snow is given in (2).

The objective of this paper is to acquire and process a series of spectro-directional field data with respect to the particular physical snow properties. The Field Goniometer System (FIGOS) used to collect *HDRF* data was developed and designed by Sandmeier et al. (5). Grain size, snow stratigraphy, temperature and density as well as concentrations of two carbon fractions (6,7) at the surface were measured as parameters to describe the relevant influences on *HDRF* mentioned above. According to the snow cover properties met in fieldwork, the data is analysed with respect to snow wetness and sun zenith angles mainly. Grain sizes and carbon concentration are used to explain different reflectance properties among dry or wet surfaces under similar sun zenith angles.

DATA ACQUISITION METHODS

A GER3700 spectroradiometer is mounted on FIGOS as used in the field campaign. A spectralon panel by Labsphere Inc. was used as reference standard. Direct and diffuse irradiation during goniometer measurements were evaluated with a YES MFR-7 solar photometer (8). To estimate the physical parameters of the snow cover, a snow pit was dug for each measuring day and samples of the top layers were taken to the cold lab to determine grain size (9). To quantify soot pollution, thermal carbon measurements (6,7) were made on snow samples taken directly from the surface. The half-hour measurements of the automatic IMIS-meteostation (Intercantonal Measuring and Information System) named ‘Fluelastrasse’ at the measurement site delivered further data to assess alterations of snow cover during the day.

Field Goniometer System (FIGOS)

The FIGOS consists of an azimuth arc of 2 m of radius on which a zenith semi-arc of the same radius is mounted, as shown in Figure 1. The sensor is fixed on a motorised sledge, which allows measurements to a maximum observation zenith angle of θ_r=75°. The single directional measurements are placed in a grid of 15° spacing in zenith direction and 30° in azimuth direction. Each hemisphere contains approximately 66 measurements of the target, and is supplemented with seven reference measurements. The goniometer has to be transported on a trailer, which strongly reduces its mobility in mountain areas. It weighs 230 kg in total and its two-hour assembly time requires two people at least.

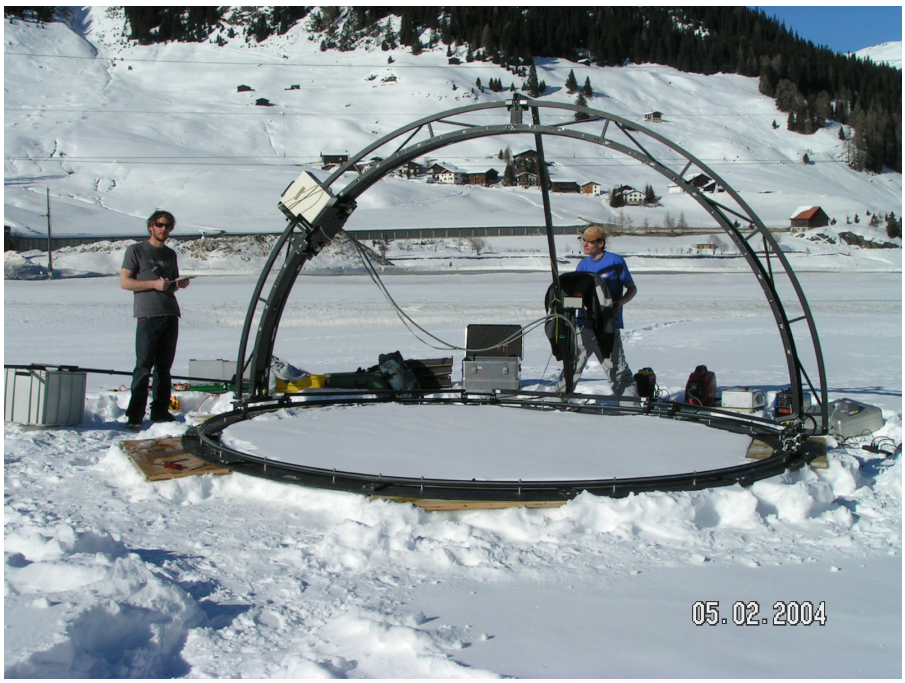

Figure 1: FIGOS-measurement performed on February 5, the first day of field campaign. Due to its weight, the goniometer was placed on wooden boards to avoid sinking.

The GER3700 spectroradiometer measures in the spectral range of λ=0.4 to 2.5 μm with a spectral resolution of 1.5 to 8.6 nm. Measured reflected radiance from target under unknown hemispherical illumination in DN is divided by the lambertian reflectance measured from spectralon panel, which also depends on unknown hemispherical illumination. The hemispherical-directional reflectance factor of the target is then calculated with the known directional reflectance characteristics of the spectralon reference panel R_{ref} (10,11) for each angle measured.

$$R_{HDRF}(\theta_i,\varphi_i;\theta_r,\varphi_r) = \frac{L_r(\theta_i,\varphi_i;\theta_r,\varphi_r)}{L_{r,lam}(\theta_i,\varphi_i)} \cdot R_{ref}(\theta_i,\varphi_i;\theta_r,\varphi_r) \quad (1)$$

In parallel to the spectro-directional data survey, the total, diffuse and direct component of the solar irradiation is being determined by a MFR-7 sun photometer. The MFR-7 measures the diffuse and the total irradiation in one panchromatic and six monochromatic bands at 415, 500, 615, 673, 870 and 940 nm, of which the direct irradiation and finally the atmospheric thickness is calculated.

Collection and analysis of snow physical parameters

For the characterisation of relevant snow physical parameters, a snow pit was dug within 15 meters of the goniometer's location. Stratigraphic characteristics such as hardness, density, temperature, and size of the snow grains as well as concentration of two carbon fractions were measured. The hardness was determined using the hand test method (12). To every layer a result of the five-level scale will be assigned. To measure snow density, a tube was run through a layer vertically to obtain a layer snow sample, which was weighed. The density is calculated with the weight and the volume given by the thickness of the layer and the tube's diameter. A digital thermometer was used to measure the snow temperatures. A first measurement was taken immediately below the surface of the snow. Because such hand-measurements are prone to radiation errors, the local snow surface temperature as obtained from the IMIS infrared sensor (see below), is a better representation of the snow surface temperature. Underneath, further measurements at distances of 5 cm followed down to a depth of 30 cm, where two more measurements were taken at a distance of 10 cm. The grain size of the snow crystals of the individual layers was determined with a simple microscopic method (3,9). For this purpose, samples were taken from the top layers of the snow pit and conserved in cooled Isooctane at the cold laboratory. The evaluation of individual snow grains was done by digital image analysis of microscopic digital photographs. Pictures of separated snow grains were taken as shown by the example in Figure 2.

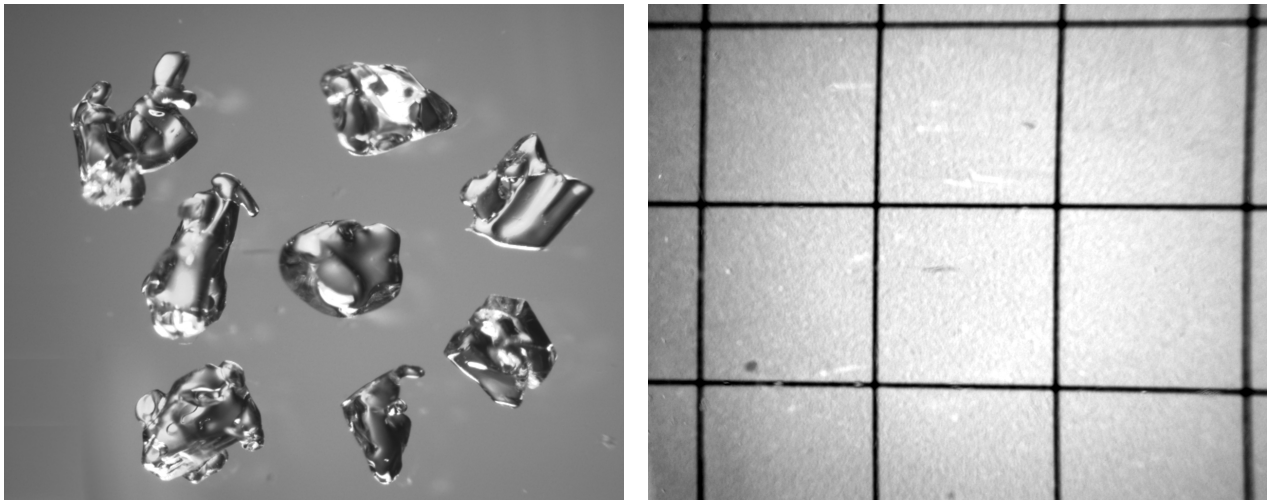

Figure 2: Microscopic digital photographs of snow grains (left, sample from March 18th, layer at 9-12 cm depth) and the reference grid (right, 2mm grid size).

A 2-mm grid was photographed as a reference to estimate the size of the grains. The image analysis programme ImagePro by Media Cybernetics, Inc. calculates a number of two-dimensional size parameters. The minimal grain radii were chosen to represent the effective grain size. As found by

Aoki et al. (3), this approach is likely to overestimate the optically equivalent grain sizes by a factor of 1.6 to 2.6.

To quantify the contamination of the snow covers, measurements of two different carbon concentrations were made at the PSI (Paul Scherrer Institute, Villigen) with samples of approximately 100 to 250 g taken from the top 5 cm of the surfaces. The samples were melted, filtered and burned at 340°C and 650°C. The CO_2 released at the two temperatures finally corresponds to organic (OC) and elemental fractions (EC).

From the data of the IMIS station of the winter 03/04, air and snow surface temperatures, snow temperatures at various depths of the snow cover and the seasonal change in the height of snow have been considered as supplementary data sources.

Field measurements

From February 5th to March 30th, 16 complete hemispheric measurements were taken. The characteristics of the snow surfaces over all measuring days show a large variability regarding snow wetness, sun zenith angle and contamination. The spectral and directional evaluations are focused on these parameters' influence on reflectance properties.

An overview of directional data and snow physical parameters is given in Table 1. The sun zenith angle θ_i and azimuth angle φ_i were evaluated from the average of the respective starting and ending time, which are given as local time. The contamination is given in elemental (EC) and organic (OC) fraction. Due to errors in measurement, results in brackets are affected by an increased uncertainty. On March 18th, a large particle of natural but unknown origin found in the snow sample makes the OC measurement less representative, though snow age and the EC measurement indicate a high value for the OC fraction, too. The amount of uncertainty cannot be estimated for the carbon measurements of February 5th. The total optical thickness of atmosphere was measured with an MFR-7 sun photometer. For measurement 0328 A, it can be assumed to be in the range of 0.14 to 0.22 rather than the value given in the table, which is explained by a sloping position of the measurement device due to sinking in the snow.

Table 1: Summary of the 16 evaluated hemispheres named after the dates of measurement in the first column.

Hemi-sphere	Starting Time	Ending Time	Avg. θ_i /°	Avg. φ_i /°	Mean grain sizes /mm	EC / μg C/l	OC / μg C/l	Total optical thickness of the atmosphere, $\tau_{(500\ nm)}$
0205 A	13.31	14.20	65.5	201.4	0.22-0.28	(643.7)	(556.9)	~0.15
0217 C	15.46	16.24	75.3	233.5	0.21-0.24	253.8	1426.8	~0.14
0303 A	11.59	12.47	53.9	176.5	0.21-0.30	64.7	1116.1	0.15-0.22
0303 B	13.47	14.15	56.9	205.4	0.21-0.30	64.7	1116.1	0.13-0.18
0303 C	15.22	15.59	67.8	231.5	0.21-0.30	64.7	1116.1	~0.11
0303 D	16.05	16.38	73.6	240.4	0.21-0.30	64.7	1116.1	~0.10
0318 A	12.05	12.45	47.9	178.6	n.a. (wet)	156.8	(4217.5)	n.a.
0318 B	13.45	14.25	52.2	210.9	n.a. (wet)	156.8	(4217.5)	n.a.
0318 C	15.20	16.20	64.5	237.4	n.a. (wet)	156.8	(4217.5)	0.20-0.45
0328 A	14.15	14.57	46.5	204.4	0.32-0.33	110.5	617.8	(0.24-0.27)
0328 B	15.50	16.33	56.6	232.2	0.32-0.33	110.5	617.8	~0.15
0329 B	11.48	12.18	47.0	151.3	n.a. (wet)	138.5	774.4	0.14-0.16
0329 C	13.17	13.41	43.4	181.2	n.a. (wet)	138.5	774.4	0.10-0.12
0329 D	14.28	14.55	46.4	206.6	n.a. (wet)	138.5	774.4	~0.09
0329 E	16.07	16.40	57.7	235.2	n.a. (wet)	138.5	774.4	~0.08
0330 D	16.14	16.43	58.4	237.1	n.a. (wet)	n.a.	n.a.	0.14-0.25

The sampled snow grains mainly consist of destructively metamorphosed crystals. The grains of

February 5th and 17th are rounded and small at the surface. While the rounding through metamorphosis increases with depth, grain sizes stay constant. The snow pit dug on March 3rd is similar to those dug in February, but with a thin layer of small dendritic remnants on top. The snow grains sampled on March 28th are of shapes similar to those sampled on March 3rd but are of a larger size. Melting metamorphosis and high liquid water content influenced the samples of the three other snow pits. Their conservation in cooled Isooctane caused refreezing of the liquid water surrounding single crystals and building grain clusters. This leads to an uncertain grain size determination where water refreezes on single grains. Image analysis for these layers revealed grain radii of up to one millimetre (Figure 3). The grain clusters in the superior layers of March 18th, 29th and 30th could not be analysed at all because of the liquid water contents being too high, as indicated in Figure 3.

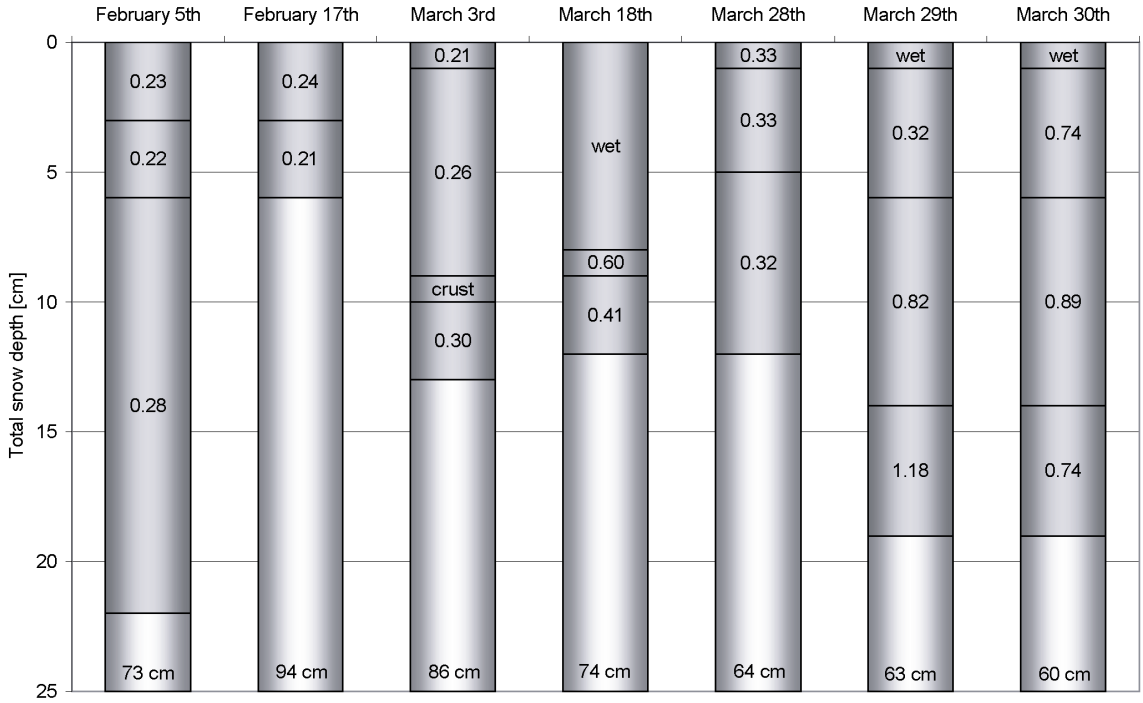

Figure 3: Grain sizes (in mm) per layer and measurement day, measured through image analysis. The total snow depth of each snow pit is indicated at the bottom of the columns. No samples could be taken from the wet surfaces on March 18th, 29th and 30th and the results of deeper layers are uncertain due to refreezing of pore water in cooled Isooctane.

ANALYSIS OF DIRECTIONAL DATA

Spectral Albedo

The spectral albedo was evaluated through hemispherical integration of the measured *HDRF* of each dataset. In the visible wavelengths, the albedo is between 70 and 95 % and then significantly decreases to values from 5 to 25% at λ = 1,500 nm. A large peak is found at some wavelength around λ=1,850 nm (Figure 4), but cannot be located precisely due to the unsteady behaviour of the GER3700 between λ=1,840 nm and λ = 1,950 nm, where the transition of the two PbS-detectors leads to insufficient SNR (13). A second peak is at λ = 2,250 nm (Figure 5). Both peaks in the infrared wavelengths seem significantly more distinctive in dry snow than in wet snow, whereas the reflectances at λ = 1,850 nm have to be considered imprecise. With few exceptions, the albedo of dry surfaces is higher than for wet surfaces at all wavelengths. For longer wavelengths, this is explained by the pore water, which increases the optically equivalent grain size, leading to a decrease in reflectance. The refreezing of wet snow conserves such increases in grain size as well as the decrease in reflectance (14). Among the dry surfaces, the measurements of

March 28th have the lowest albedo, as expected due to the higher absorption caused by the slightly larger grain sizes (15). A correlation of the measured carbon fractions and the albedo at the shorter wavelengths is not obvious. However, in the measurement at the largest sun zenith angles, an exceptional decrease of the albedo at the shorter wavelengths is observed. The measurements of March 18th with the highest carbon contaminations show an exceptional decrease in albedo at the shorter wavelengths with increasing sun zenith angle. But an expected decrease caused by the contamination (16) could not be assessed in spite of the considerable concentrations found.

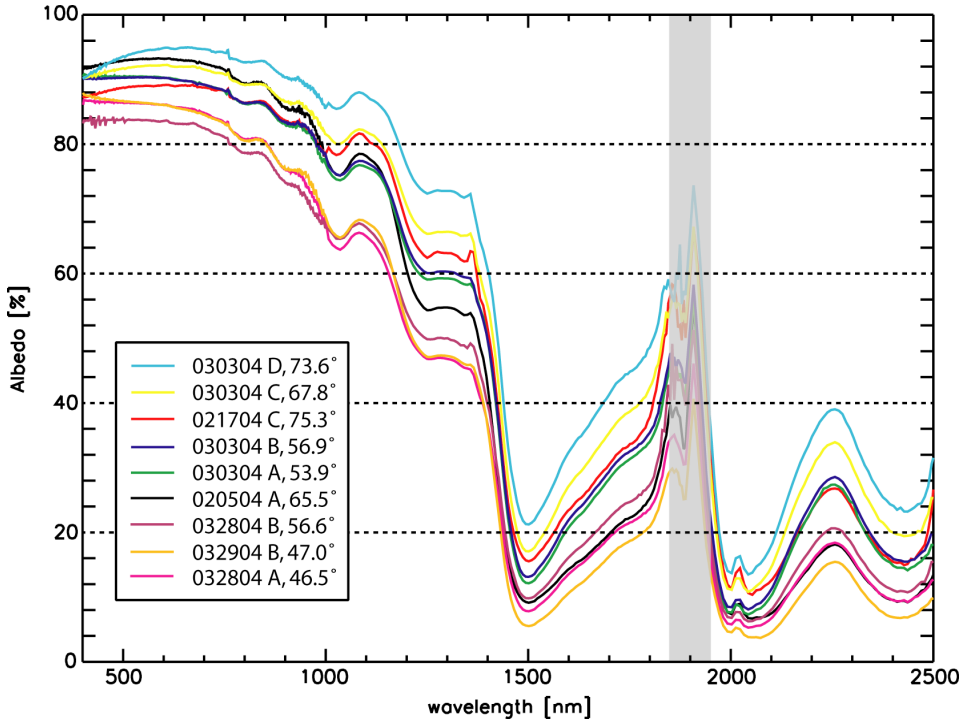

Figure 4: Spectral albedo for all dry snow surfaces. The wavelengths 1,840 to 1,950 nm indicated with a grey bar are affected by bad SNR as described at the beginning of section 'spectral albedo'.

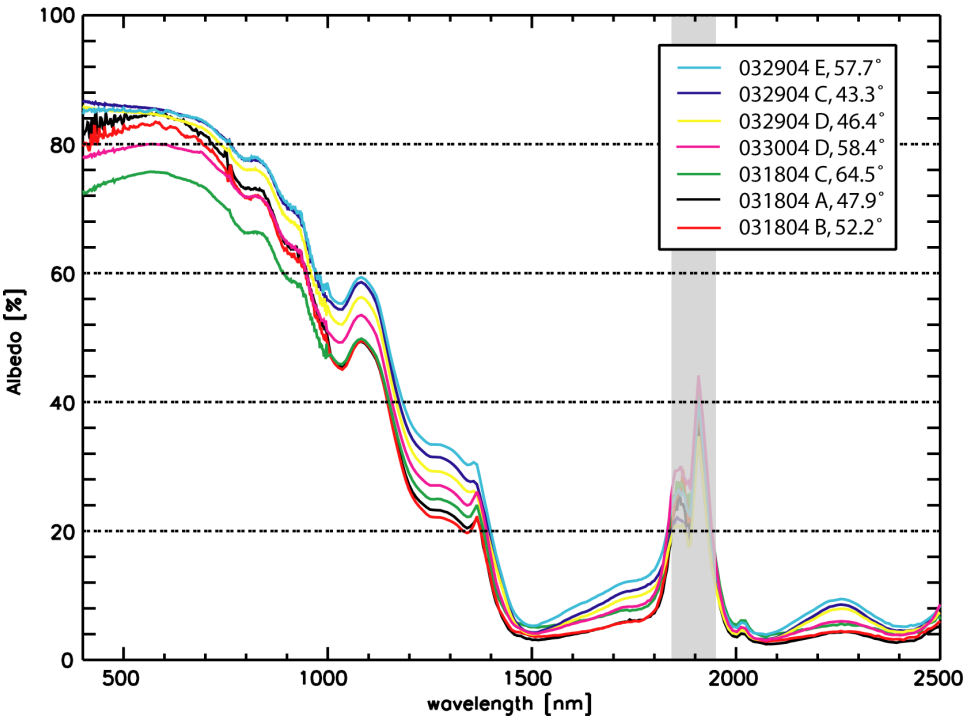

Figure 5: Spectral albedo for all wet snow surfaces. The wavelengths 1,840 to 1,950 nm indicated with a grey bar are affected by bad SNR as described at the beginning of section 'spectral albedo'.

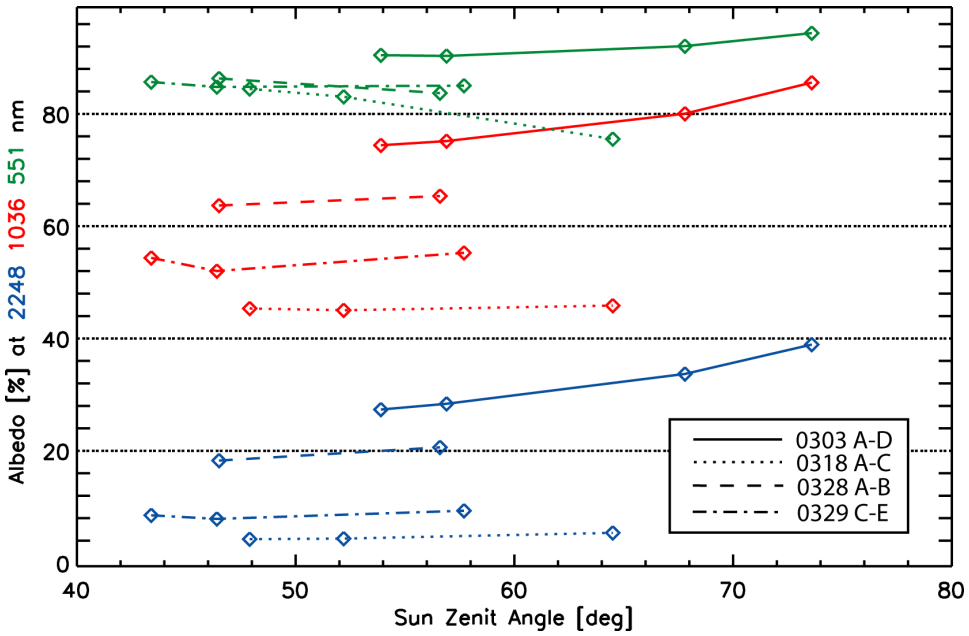

Figure 6: Alteration of the albedo with sun zenith angle at three wavelengths for four measuring days. The 0329 B is not included, as it took place before the melting metamorphosis started and therefore has a higher albedo than the afternoon measurements.

Previous work raises the question of whether the albedo of snow increases with increasing sun zenith angle (15). Figure 6 shows that an increase of the albedo with the sun zenith angle can only be stated in the four measurements of March 3rd. On March 18th, the short-wave albedo even significantly decreases with increasing sun zenith angle. A possible explanation is that the pollution is concentrated superficially as assumed by Aoki et al. (3) to match their field data with model results. In this case, the short-wave absorption through superficial contamination might be increased as the vertical penetration depth decreases with increasing sun zenith angle. An analogous explanation can be given due to the wet snow layer. While its thickness might not affect the reflectances at longer wavelengths because infrared light does not reach the relevant depth, it could have an influence on the short-wave radiation.

Directional Reflectance

To assess the anisotropy factors (*ANIF*) of the spectral directional data, the directional reflectance spectra is normalised with spectral albedo (17):

$$ANIF(\lambda;\theta_i,\varphi_i;\theta_r,\varphi_r) = \frac{R_{HDRF}(\lambda;\theta_i,\varphi_i;\theta_r,\varphi_r)}{\alpha(\lambda;\theta_i,\varphi_i)} \quad (2)$$

where R_{HDRF} is hemispherical directional reflectance, α is spectral albedo, θ_i and φ_i are the sun zenith and azimuth angles, θ_r and φ_r are observation zenith and azimuth angles, respectively.

To compare the anisotropy among the hemispheres we chose the *ANIF* of the maximum forward scattering direction (θ_r = 75°, φ_r = 0°), as shown in Figure 7 and 8. The albedo normalised *ANIF* depends on the snow surface properties, sun zenith angle and the ratio of direct to diffuse illumination. The analysis was performed with respect to snow surface properties and sun zenith angle. The influence of illumination is neglected, although it reaches considerable variation especially on March 18th, as given in Table 1.

The wet snow surfaces with θ_i = 43.3 to 64.5° were measured at smaller sun zenith angles than the dry ones with θ_i = 46.5 to 75.3°, but have similar *ANIF*. Thus, anisotropy is higher for wet surfaces. This observation agrees with the results of Dozier et al. (14), who found that anisotropy increases with sun zenith angle, grain size (or the similar optical effect caused by pore water) and wavelength. A small influence of grain sizes can be estimated based on the measurements 0328 B (0.32 - 0.33 mm, homogeneous) and 0303 A and B (0.21 mm on the surface up to 0.30 mm at

10 cm depth). At λ = 1,500 nm, 0328 B has an *ANIF* of 6.7. 0303 B has a sun zenith angle only 0.3° larger than 0328 B, but the *ANIF* at the same wavelength amounts to a value of 5.2. This difference appears also with the peaks at λ = 2.07 μm. The reason for that is considered to be the slightly smaller grain size. 0303 A refers to the same snow surface at a 3° smaller sun zenith angle. With that decrease, the *ANIF* decreases to 4.

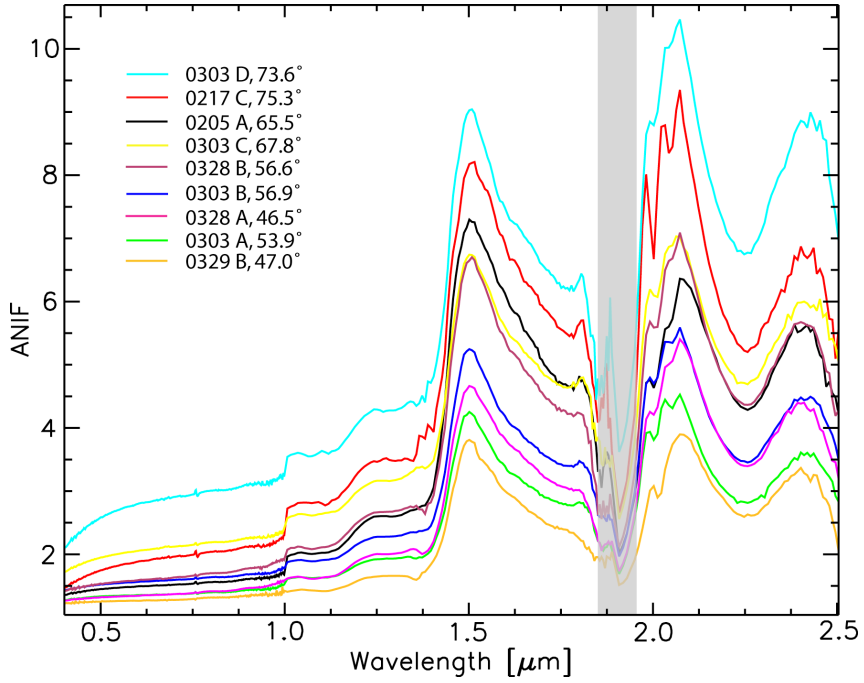

Figure 7: The albedo-normalised ANIF *of the reflectance maxima in forward direction of the solar principal plane (θ_r=75°, φ_r=0°) for all dry hemispheres. The wavelengths 1,840 to 1,950 nm indicated with a grey bar are affected by bad SNR as described at the beginning of section 'spectral albedo'.*

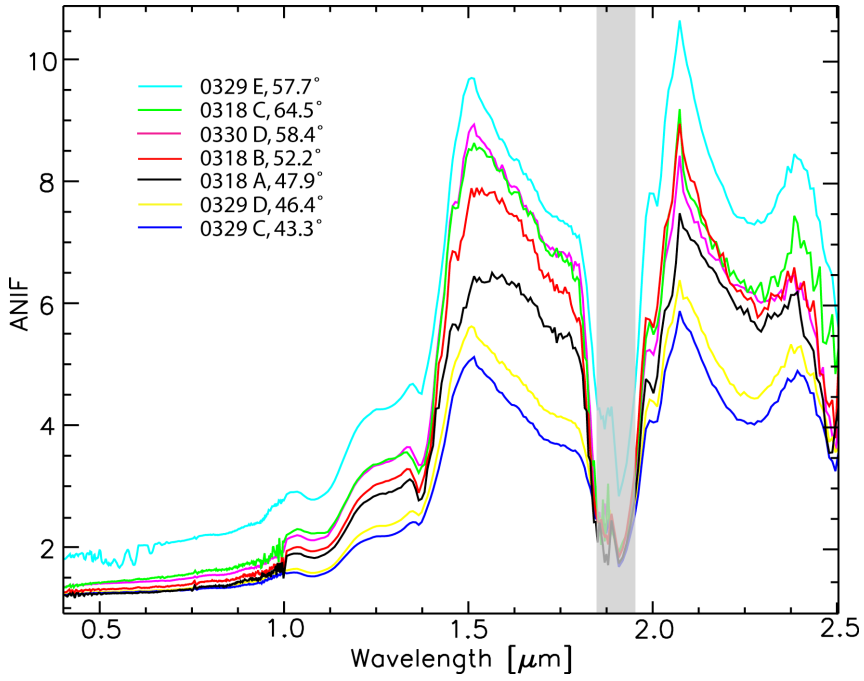

Figure 8: The albedo-normalised ANIF *of the reflectance maxima in forward direction of the solar principal plane θ_r=75°, φ_r=0°) for all wet hemispheres. The wavelengths 1,840 to 1,950 nm indicated with a grey bar are affected by bad SNR as described at the beginning of section 'spectral albedo'.*

The snow surfaces of March 18th, the day with the most intensive melting metamorphosis, show slightly different characteristics than the other wet snow surfaces, mainly at the wavelengths 1,500 to 1,800 nm. They are more irregular in shape and the local maximum seems to have slightly shifted towards the longer wavelengths. In addition, the maximum at 2,070 nm is slightly wider with wet surfaces. A possible explanation comes from preferential flow paths and large agglomerates of grains, which both create variability in the thick melting layer.

On all measuring days the anisotropy increased with increasing sun zenith angle as shown in Figure 9, with few exceptions at short wavelengths. The increase of *ANIF* at smaller wavelengths is small, but strongly increasing with wavelength. An analysis of the *ANIF* at θ_r = 75°, φ_r = 0° for the measuring days with several measured hemispheres shows that this effect is stronger with the wet surfaces on March 3rd. Although measurements with large sun zenith angles are lacking for this day, maxima in forward direction of the solar main plane are reached up to *ANIF*=10 at θ_l = 57.7°.

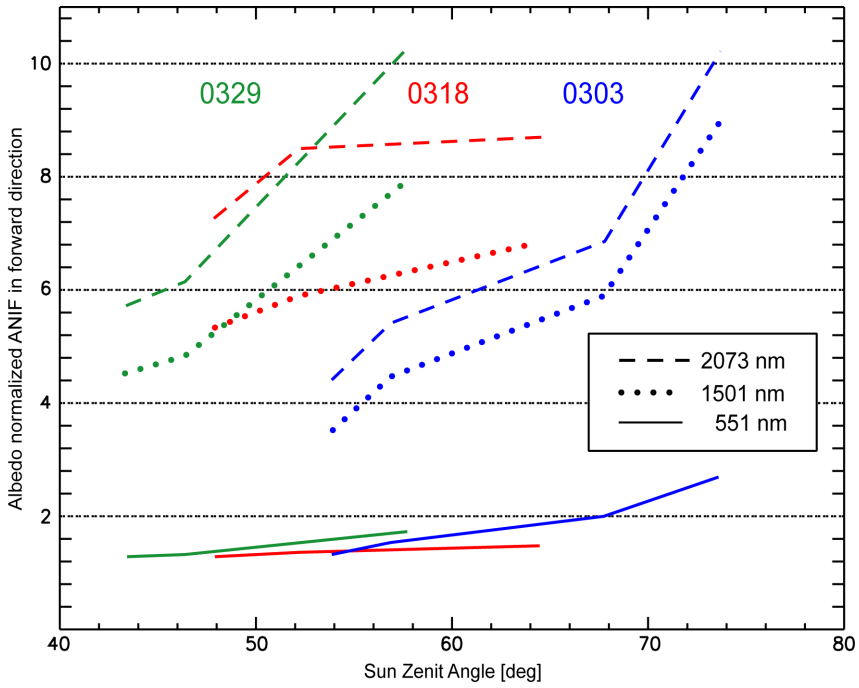

Figure 9: ANIF *in view direction* θ_r*= 75° and* φ_r*= 0° for* λ*=551, 1,501 and 2,071 nm. Three measurements each of March 18th and 29th (wet), as well as four of March 3rd (dry) are shown.*

While the anisotropy for the measurements of March 29th and March 3rd increases similarly with sun zenith angle, the increase on March 18th, the day with the most intensive melting metamorphosis, is smaller at all wavelengths. This suggests that the wetness causes an increase of the anisotropy but, on the other hand, the increase with the sun zenith angle is reduced.

Spectral reflectance of dry and wet snow surfaces

The spectral differentiation of dry and wet snow was examined referring to model results of previous work (18), which suggest the wavelengths λ=980 and 1,030 nm to be suitable for distinction. The nadir directions of all measured hemispheres indicate a sufficient differentiability at the wavelengths mentioned. Though, the differentiability decreases with increasing view zenith angle, because the dissimilarity among the twelve azimuth view angles increases with the zenith angle due to the forward scattering of snow. To determine the ideal wavelength for the present data, the data scanned along azimuth direction of each zenith angle were averaged. Groups with view zenith angles θ_r=0, 15, 30, 45 and 60° were formed of the spectra of dry surfaces as well as of the spectra of wet surfaces. For each view zenith angle the mean reflectance of the wet surfaces and both standard deviations were subtracted from the mean reflectance of the dry surfaces:

$$\Delta R(\lambda, \theta_r) = \left(\overline{R}_{dry} - \overline{R}_{wet}\right) - \left(\sigma_{R_{dry}} + \sigma_{R_{wet}}\right) \quad (3)$$

where $\overline{R}_{dry}$ and $\overline{R}_{wet}$ are the mean reflectances of dry and wet surfaces, respectively; and σ_{Rdry} and σ_{Rwet} are the standard deviations of the reflectances of dry and wet surfaces, respectively. The sum $\sigma_{Rdry} + \sigma_{Rwet}$ gives an amount of variation by which the reflectances $\overline{R}_{dry}$ and $\overline{R}_{wet}$ have to differ in order to allow a differentiation with a 95% confidence interval. Thus, those values have a statistical rather than a physical meaning.

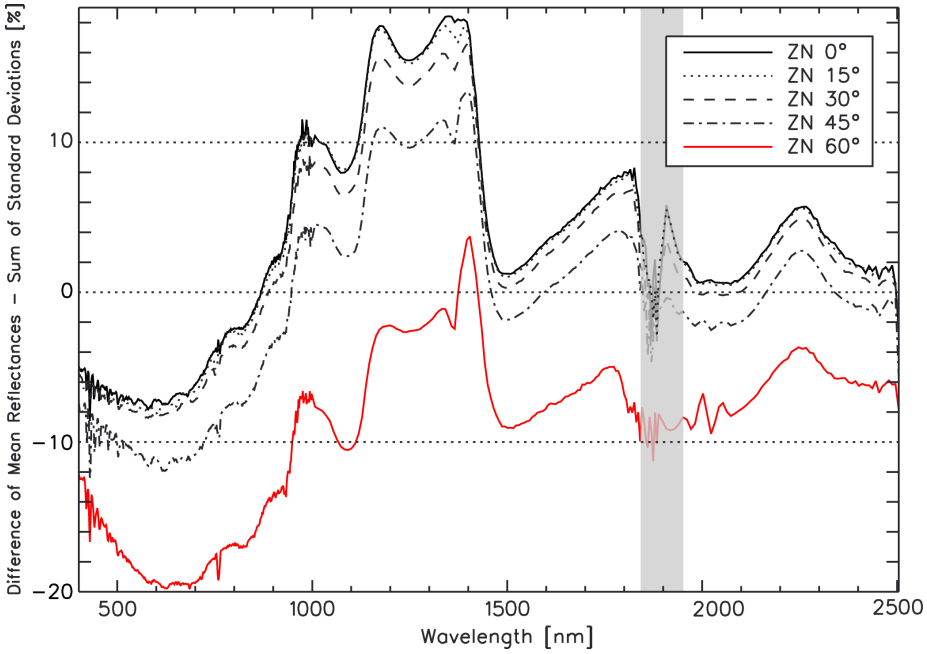

Figure 10: For dry and wet measurements, the average of all spectra was calculated for each observation zenith angle θ_r= 0 to 60°. The average reflectance spectrums of wet and dry snow were subtracted and reduced by both standard deviations for the mean reflectance of dry and wet snow. The wavelengths 1,840 to 1,950 nm indicated with a grey bar are affected by bad SNR as described at the beginning of section 'spectral albedo'.

Figure 10 clearly shows the decrease in differentiability with increasing view zenith angle. At the value zero, only measurements within the standard deviations are classified correctly. Negative values indicate even worse differentiability. The figure shows a local maximum at λ =1,000 nm, in which the ice and water absorption bands do not develop clear peaks as expected (18). A better differentiability appears at λ =1,150 to 1,380 nm. A clear maximum for increasing zenith angles is visible at the water absorption band at 1,380 nm, where the decrease of reflectance is greatest due to wetness. Different characteristics between dry and wet surfaces in this bandwidth can also be recognised while comparing the albedo.

Problems in adequate data acquisition

The determination of snow physical parameters as done in this work is of qualitative character and the measurement values could therefore not be correlated quantitatively with directional reflectance properties. Especially the measurement of snow grain sizes has to be done with higher accuracy and with respect to snow grain shape. Differences of a tenth millimetre have significant influence on *HDRF*. The accuracy of the method used is assumed to be too low to meet such requirements. Furthermore, snow physical parameters change considerably during cloudless days with temperatures around 0°C, a one-time collection as performed might not be sufficient if a higher accuracy is necessary.

SNR of GER3700 is insufficient at wavelengths from λ=1,840 to 1,950 nm (13), where the transition of the two PbS-detectors is situated. This problem has to be solved to analyse the reflectance

peak at λ=1,850 nm. The SNR is only slightly affected by low signal in other atmospheric absorption bands, where the spectroradiometer measures regularly.

CONCLUSIONS

Many characteristics of the bidirectional reflectance distribution function (*BRDF*) suggested by previous work could be confirmed by our measured *HDRF* data: Albedo decreases with increasing grain size and wavelength or due to snow wetness. Anisotropy increases with increasing grain size, sun zenith angle, wavelength or due to snow wetness. Highest anisotropy for all hemispheres is found in forward direction, monotonically increasing with zenith angle up to the largest angle measured in this study at θ_r=75°. Otherwise, no significant conclusion can be made regarding the influence of the sun zenith angle on snow albedo. The effect of the measured carbon concentrations is not significant by comparing *HDRF* measurements of different surfaces, although concentrations vary up to a factor of 4 as far as OC is concerned. For the spectral differentiation of wet and dry snow, the spectral feature at λ = 1,380 nm is suggested to be the most suitable wavelength.

As far as snow contamination is concerned, no proper correlation was found. The effect is probably of smaller magnitude than that caused by variation of snow grain size. A more accurate differentiation of pollutants might be necessary to find a correlation of contamination and albedo.

Future analysis of snow *HDRF* should cover a larger variety of grain size and morphology. Since snow reflectance properties are sensitive to small changes in optically equivalent grain size, a more accurate method is needed for parameterisation. Furthermore, a method to quantify liquid water content and to describe the optically equivalent grain size of wet snow is necessary to investigate spectrodirectional effects quantitatively.

ACKNOWLEDGEMENTS

We thank Andreas Eisele, Rosey Grant, Nora Helbig, Beni Müller (Swiss Federal Institute for Snow and Avalanche Research); Isabella Flüeler, Chrigi Gemperle, Stephan Hayoz, Jamil Mokhtar, Tania Rodriguez, Martin Scherler (University of Zurich, Department of Geography); and Saskia Bourgeois (Swiss Federal Institute of Technology, Institute for Atmospheric and Climate Science, Zürich), for their assistance in the field campaign, which made this work possible at all.

REFERENCES

1 Nicodemus F E, J C Richmond, J J Hsia, I W Ginsberg & T Limperis, 1977: Geometrical considerations and nomenclature for reflectance. National Bureau of Standards, U.S. Department of Commerce, Vol. NBS Monograph 160, 67 pp.

2 Painter T H & J Dozier, 2004. Measurements of the hemispherical-directional reflectance of snow at fine spectral and angular resolution, In: Journal of Geophysical Research (Atmospheres), Vol. 109, D18115, doi:10.1029/2003JD004458

3 Aoki T, M Fukabori, A Hachikubo, Y Tachibana & F Nishio, 2000. Effects of snow physical parameters on spectral albedo and bidirectional reflectance of snow surface. Journal of Geophysical Research, Vol. 105(D8): 10219-10236

4 Warren S G, R E Brandt & P O'Rawe Hinton, 1998. Effect of surface roughness on bidirectional reflectance of Antarctic snow. Journal of Geophysical Research (Planets), Vol. 103: 25,789-25,807

5 Sandmeier S R, W Sandmeier, K I Itten, M E Schaepman & T W Kellenberger, 1995. The Swiss Field Goniometer System (FIGOS). Proceedings of IGARSS '95 (Firenze, Italy) 2078-2080

6 Cachier H, M P Bremond & P Buat-Ménard, 1989. Determination of atmospheric soot carbon with a simple thermal method. Tellus, 41B: 379-390

7 Lavanchy V M H, H W Gaggeler, S Nyeki & U Baltensperger, 1999. Elemental Carbon (EC) and Black Carbon (BC) measurements with a thermal method and an aetholometer at the high-alpine research station Jungfraujoch. Atmospheric Environment, 33: 2759-2769

8 MFR-7, 2002. Multi-Filter Rotating Shadow Band Radiometer Model MFR-7, bulletin MFRSR-7, Yankee Environmental Systems Inc., 6 pp.

9 Brun E & E Pahaut, 1991. An efficient method for a delayed and accurate characterization of snow grains from natural snowpacks. Journal of Glaciology, 37(127): 420-422

10 Labsphere Calibration Data, 1995. Reflectance Calibration Standards, Report-No. 13610-A, US-North Sutton (NH 03260) 4 pp.

11 Sandmeier S E & K I Itten, 1997. A physically-based model to correct atmospheric and illumination effects in optical satellite data of rugged terrain. IEEE Transactions on Geoscience and Remote Sensing, 35(3): 708-717

12 Munter W, 1999. 3 x 3 Lawinen: Entscheiden in kritischen Situationen. Agentur Pohl & Schellhammer, Edition VIVALPIN, ISBN 3-00-002060-8, 87-88

13 Schaepman M E, 1998. Calibration of a field spectroradiometer – Calibration and characterization of a non-imaging field spectroradiometer supporting imaging spectrometer validation and hyperspectral sensor modelling. RSL Remote Sensing Series, Vol. 31, 146 pp.

14 Dozier J, R E Davis, A T C Chang & K Brown, 1988. The spectral bidirectional reflectance of snow. In: 4th International Colloquium on Spectral Signatures of Objects in Remote Sensing (Aussois, France) 87-92

15 Warren S G, 1982. Optical properties of snow. Reviews of Geophysics and Space Physics, 20: 67-89

16 Warren S G & W J Wiscombe, 1980. A model for the spectral albedo of snow, II, Snow containing atmospheric aerosols. Journal of the Atmospheric Sciences, 37: 2734-2745

17 Strub G, U Beisl, M E Schaepman, D Schläpfer, C Dickerhof & K I Itten, 2002. Evaluation of diurnal hyperspectral HDRF data acquired with the RSL field goniometer during the DAISEX'99 campaign. ISPRS, 57: 184-193

18 Green R O, J Dozier, D A Roberts & T H Painter, 2002. Spectral snow reflectance models for grain size and liquid water fraction in melting snow for the solar reflected spectrum. Annals of Glaciology, 34: 71-73